SUPPLEMENTARY INFORMATION

A revised mechanistic model for sodium insertion in hard carbons

Heather Au,[1] Hande Alptekin,[1] Anders C.S. Jensen,[1,2] Emilia Olsson,[1,2,3] Christopher A. O'Keefe,[4] Thomas Smith,[4] Maria Crespo-Ribadeneyra,[1] Thomas F. Headen,[5] Clare P. Grey,[4] Qiong Cai,[3] Alan J. Drew[2] and Maria-Magdalena Titirici[1*]

[1]*Department of Chemical Engineering, Imperial College London, London, SW7 2AZ, UK.*

[2]*School of Physics and Astronomy and Materials Research Institute, Queen Mary University of London, London, E1 4NS, UK.*

[3]*Department of Chemical and Process Engineering, University of Surrey, Guildford, GU2 7XH, UK.*

[4]*Department of Chemistry, University of Cambridge, Cambridge, CB2 1EW, UK.*

[5]*ISIS Pulsed Neutron and Muon Source, Rutherford Appleton Laboratory, STFC, Didcot OX11 0QX, UK.*

[*]*Corresponding author.*

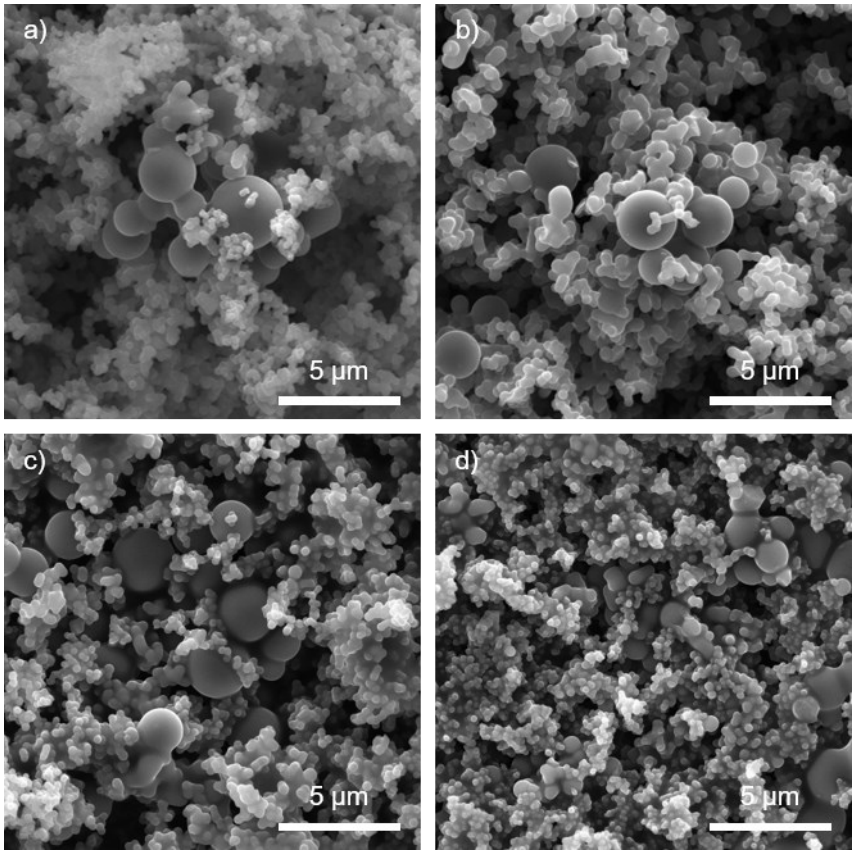

Figure S1. SEM images of a) G1000, b) G1300, c) G1700, and d) G1900.

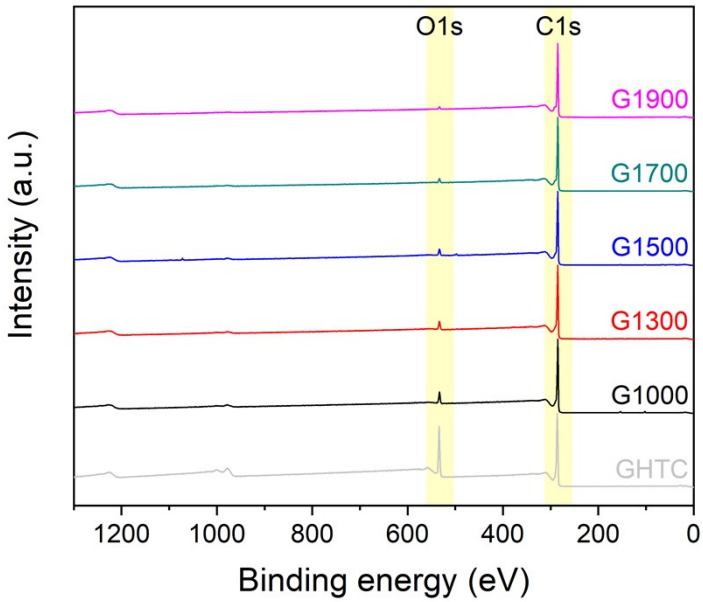

Figure S2. Wide survey XPS spectra of the materials before and after pyrolysis at each temperature.

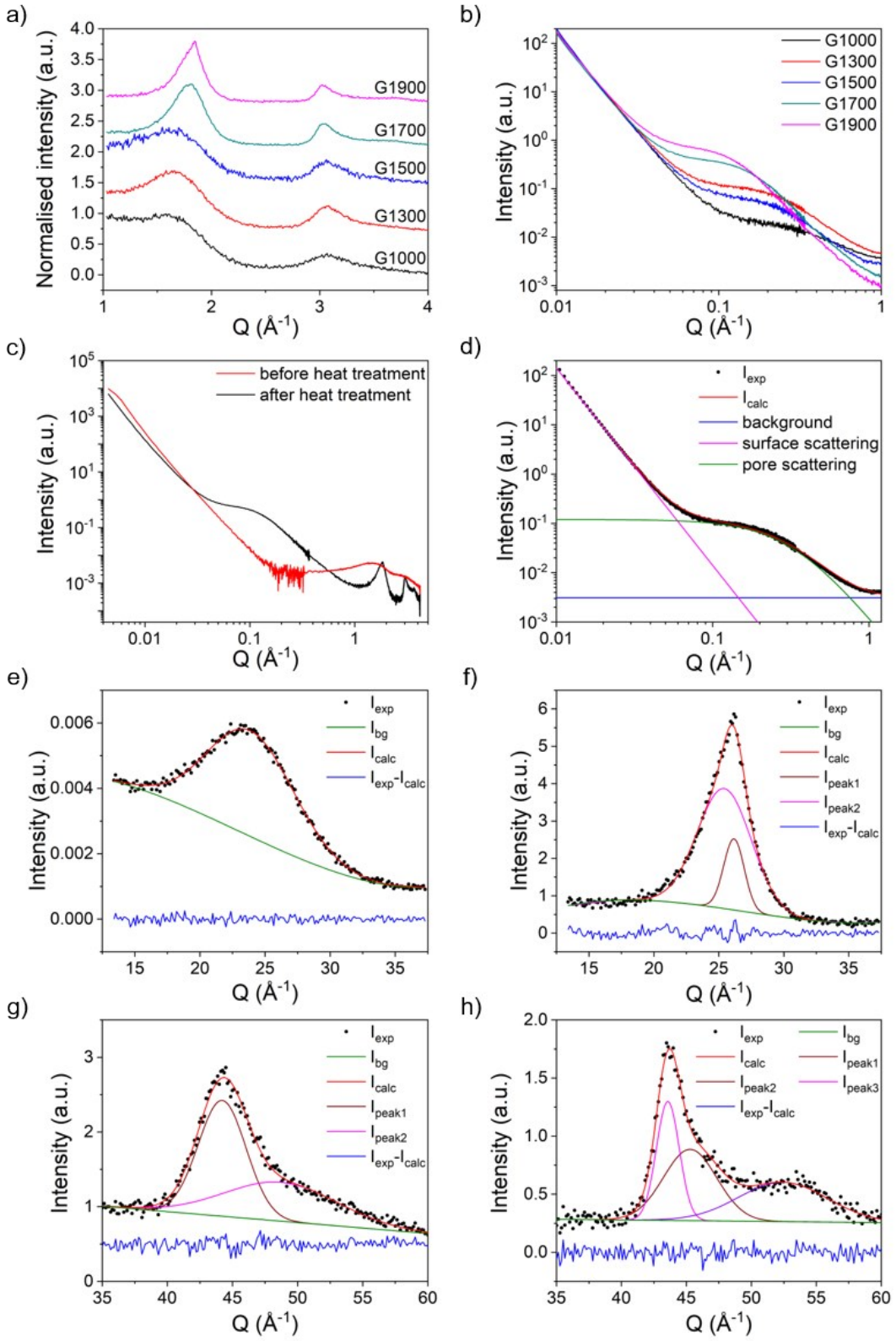

Figure S3. a) WAXS and b) SAXS data for the different samples after heating; c) comparison of the SAXS/WAXS pattern before and after pyrolysis; example fits for d) the SAXS data and the 002 peak for e) low and f) high temperature carbons, and the 100 peak for g) low and h) high temperature carbons.

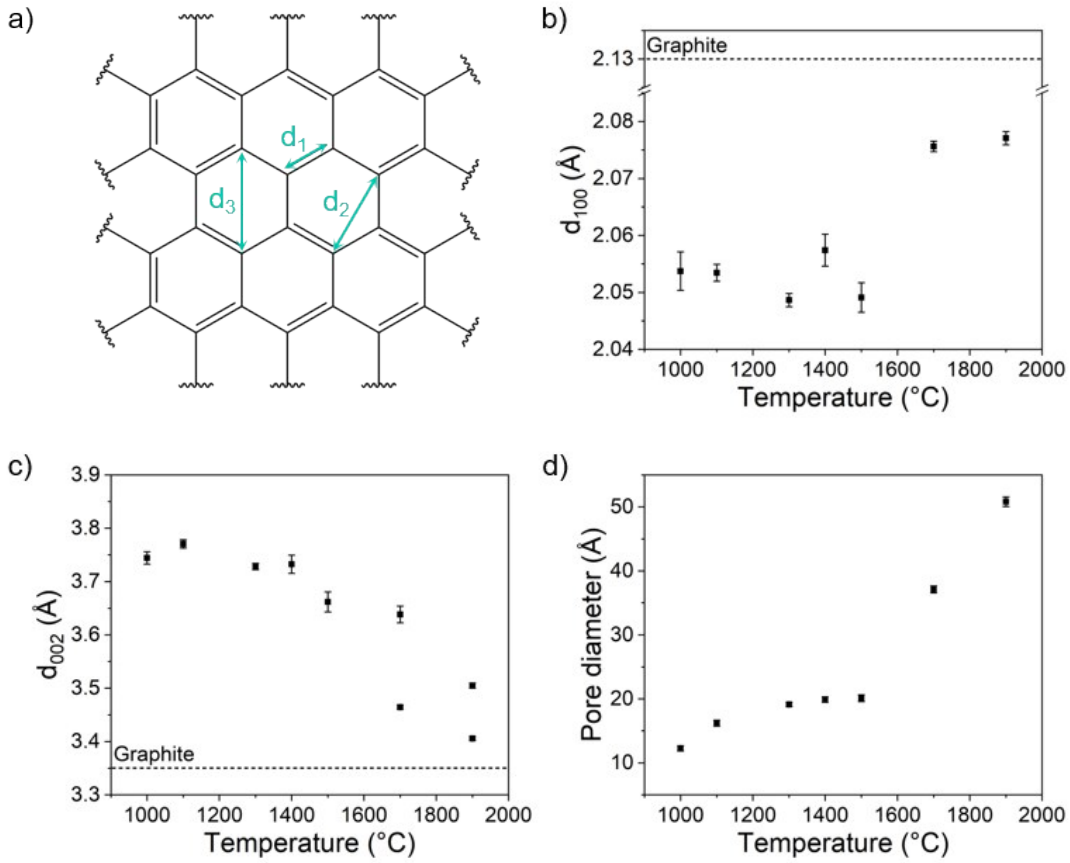

Figure S4. a) Schematic of the interatomic distances C=C (d_1), between next-nearest-neighbour carbons (d_2), and the C_1-C_4 distance in a benzene ring (d_3); b) in-plane distance calculated from the 100 peak; c) interlayer distance calculated from the 002 peak; and d) pore size calculated from the Guinier-Porod region in the SAXS range, for the carbon materials.

SAXS and SANS model:

The model described by Stevens and Dahn[1] describes a porous matrix with random size and shape of the pores and is reported in the following form:

$$I(Q) = \frac{A}{Q^4} + \frac{B' a_0^4}{\left(1 + a_0^2 Q^2\right)^2} + D \qquad \textit{(Equation S1)}$$

I(Q): scattered intensity as a function of Q,

Q: scattering vector,

A: scale factor for the surface scattering at low Q,

B': scale factor for the pore scattering, and proportional to the surface area of the pores,

a_0: size factor related to the radius of a spherical pore, R, by $a_0 = R \times 10^{-0.5}$,

D: height of the flat background.

This equation can be modified so that *B'* becomes proportional to the number of pores by adding an a_0^2 term[1] to give:

$$I(Q) = \frac{A}{Q^4} + \frac{B'' a_0^6}{\left(1 + a_0^2 Q^2\right)^2} + D \qquad \textit{(Equation S2)}$$

In a similar manner *B''* can be converted into a volume-weighted scale factor by removing an a_0^3 term to give:

$$I(Q) = \frac{A}{Q^4} + \frac{B a_0^3}{\left(1 + a_0^2 Q^2\right)^2} + D \qquad \textit{(Equation S3)}$$

Which is the equation used in this work. However, it should be noted that the contrast (i.e. the difference in scattering length density between the carbon walls and the pores) is also contained in the *B* factor and will affect the results. However, given the small change in composition between the samples, the low difference in density of the graphitic walls and the large difference in signal it should not affect the overall trend in the pore volume determined by the model.

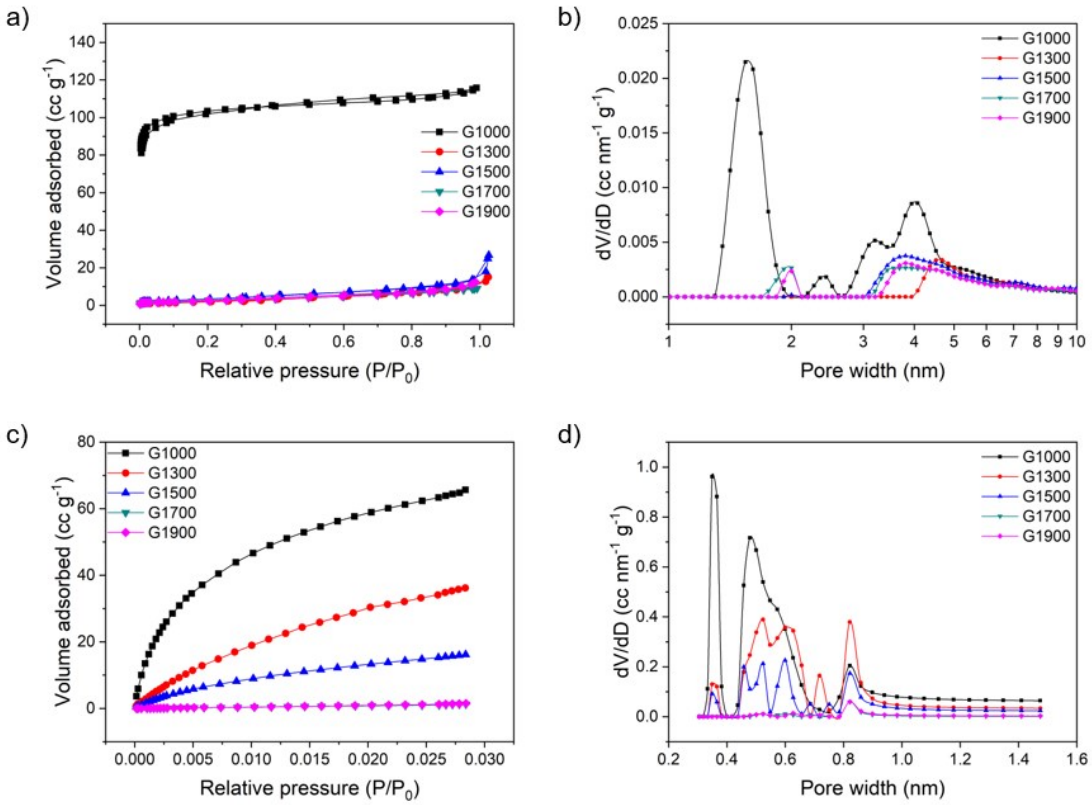

Figure S5. a) N_2 adsorption/desorption isotherms at 77 K, b) corresponding pore size distributions, c) CO_2 adsorption isotherms at 273 K, and d) corresponding pore size distributions of G1000-G1900, obtained from the adsorption isotherms based on the NLDFT method.

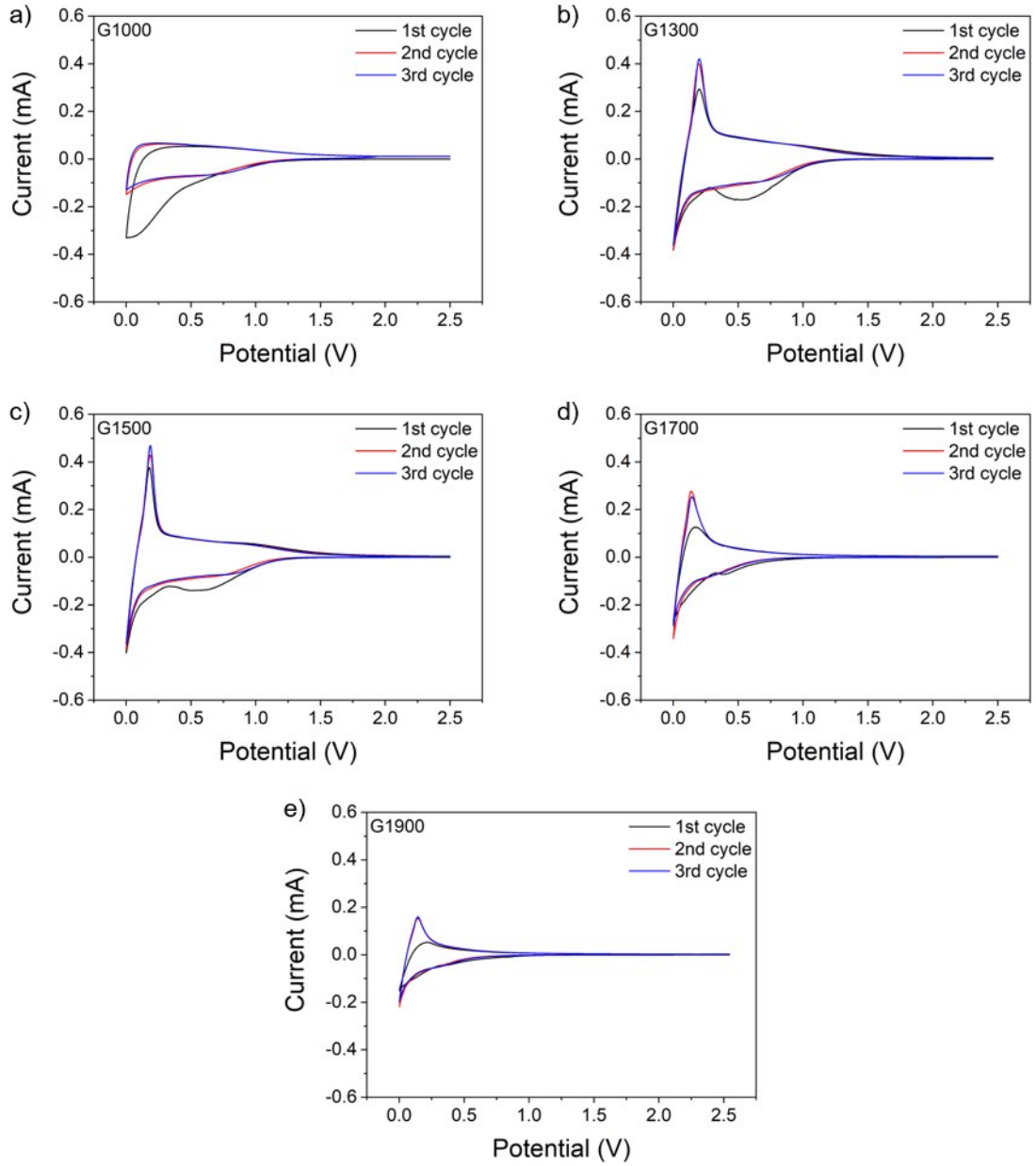

Figure S6. CV curves of a) G1000, b) G1300, c) G1500, d) G1700 and e) G1900, at 0.1 mV s^{-1}, for the first three cycles.

In the CV curves, during the first cycle as the carbon is sodiated, an irreversible process (SEI formation or sodium binding at defects) occurs between 0 and 0.7 V in G1000, and around 0.7 V for the other samples. Due to this irreversible loss of sodium, upon discharging, a smaller current flows because fewer sodium ions are able to return to the sodium electrode. In subsequent cycles, as sodiation is reversible, the oxidation current (~0.2 V) increases, matching the reduction current (~0.1 V) in intensity.

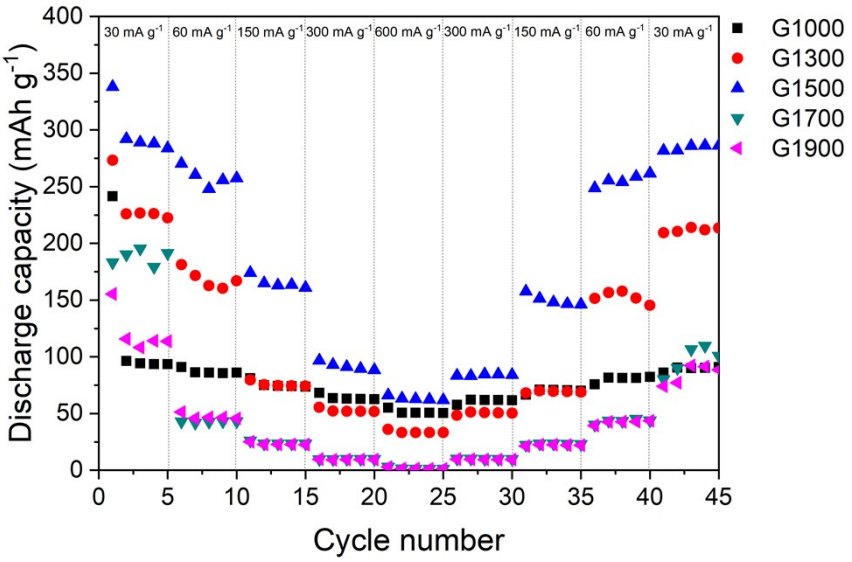

Figure S7. Rate performance of the discharge capacities of G1000, G1300, G1500, G1700 and G1900 at current densities between 30 and 600 mA g^{-1}.

When cycled at progressively higher current densities, G1500 still achieved the highest capacity of 66 mAh g^{-1} at a current density of 600 mA g^{-1}, but the performance of G1000 remained the most consistent across the range of current densities. Conversely, the high temperature materials exhibited extremely poor behaviour at high C-rates, with the capacity dropping to 1 mAh g^{-1} at 600 mA g^{-1}. This trend in rate capability may be, in part, explained by the polarisation of the reference/counter electrode in the half cell setup, where the resulting overpotential causes the cell to reach the lower cut-off potential prematurely, thus bypassing capacity at very low voltages.[2] The higher temperature materials (G1700 and G1900), which derive the bulk of their capacity from the plateau region close to 0 V, therefore exhibit far worse behaviour at higher C-rates than the lower temperature materials, which contain larger contributions from the higher potential sloping region. All the materials recovered their original capacities upon returning to 0.1C (30 mA g^{-1}), showing that the electrodes are stable even under extreme cycling conditions.

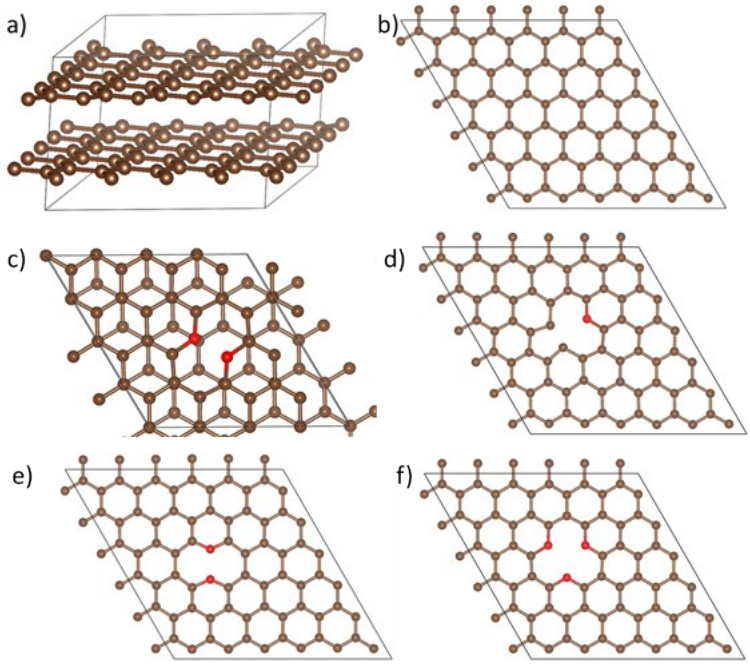

Figure S8. Schematic representation of the optimised structures for a) bilayer graphitic model, b) monolayer, c) bilayer with $2O_C$ defect, d) monolayer with O_C defect, e) monolayer with $2O_C$ defect, and f) monolayer with $3O_C$ defect. Brown spheres are carbon and red spheres are oxygen.

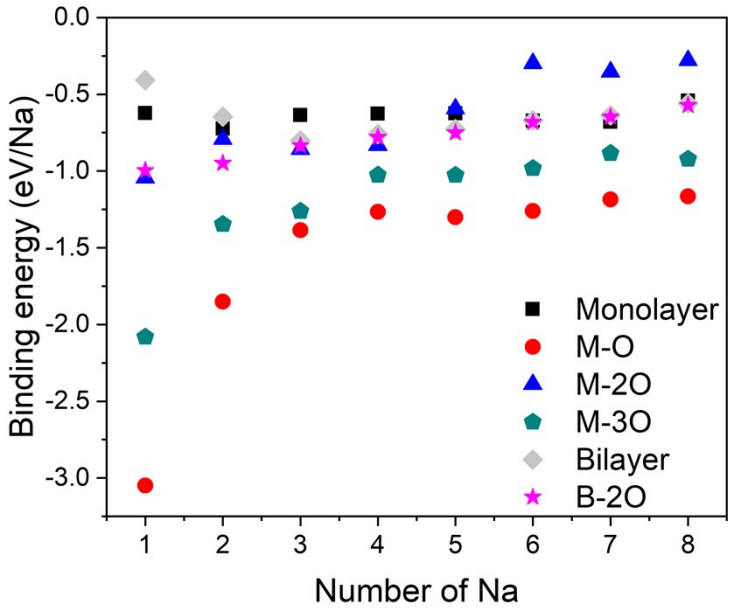

Figure S9. Simulated sodium binding energy on a pristine graphene monolayer (black squares), graphene monolayer (M) with O_C defect (red circles), $2O_C$ defect (blue triangles), $3O_C$ defect (green pentagons), in a pristine graphitic bilayer (grey diamonds), and a graphitic bilayer with a $2O_C$ defect in one layer (magenta stars).

Table S1. Pore volumes of the hard carbon materials calculated from N_2 and CO_2 adsorption isotherms.

Sample	Pore volume (N_2) (cc g^{-1})	Pore volume (CO_2) (cc g^{-1})
GHTC	-	-
G1000	0.164	0.195
G1300	0.014	0.121
G1500	0.019	0.060
G1700	0.013	0.005
G1900	0.016	0.001

Table S2. Summary of electrochemical performance and theoretical capacity for the carbon materials.

Sample	Resistivity (10^{-2} Ω m)	1st cycle capacity (mAh g^{-1})	2nd cycle capacity (mAh g^{-1})	FCCE[a] (%)	First cycle capacity		$Q_{O\text{-}defect}$[b] (mAh g^{-1})
					Slope	Plateau	
G1000	2.4	238	96	39	238	0	130
G1300	2.2	273	226	81	111	162	87
G1500	1.6	338	293	85	122	216	74
G1700	1.5	183	190	96	66	117	50
G1900	1.3	155	116	75	61	94	29

[a]*First cycle Coulombic efficiency.*
[b]*Theoretical capacity calculated assuming one sodium ion per one oxygen defect.*

References

1. Stevens DA, Dahn JR. An In Situ Small-Angle X-Ray Scattering Study of Sodium Insertion into a Nanoporous Carbon Anode Material within an Operating Electrochemical Cell. *Journal of The Electrochemical Society* **147**, 4428-4431 (2000).

2. Li Z, Jian Z, Wang X, Rodríguez-Pérez IA, Bommier C, Ji X. Hard carbon anodes of sodium-ion batteries: undervalued rate capability. *Chemical Communications* **53**, 2610-2613 (2017).